Atmos. Chem. Phys., 20, 14123–14138, 2020
https://doi.org/10.5194/acp-20-14123-2020

Atmospheric Chemistry and Physics
Open Access
EGU

Measurements of higher alkanes using NO^+ chemical ionization in PTR-ToF-MS: important contributions of higher alkanes to secondary organic aerosols in China

Chaomin Wang[1,2], Bin Yuan[1,2], Caihong Wu[1,2], Sihang Wang[1,2], Jipeng Qi[1,2], Baolin Wang[3], Zelong Wang[1,2], Weiwei Hu[4], Wei Chen[4], Chenshuo Ye[5], Wenjie Wang[5], Yele Sun[6], Chen Wang[3], Shan Huang[1,2], Wei Song[4], Xinming Wang[4], Suxia Yang[1,2], Shenyang Zhang[1,2], Wanyun Xu[7], Nan Ma[1,2], Zhanyi Zhang[1,2], Bin Jiang[1,2], Hang Su[8], Yafang Cheng[8], Xuemei Wang[1,2], and Min Shao[1,2]

[1]Institute for Environmental and Climate Research, Jinan University, 511443 Guangzhou, China
[2]Guangdong-Hongkong-Macau Joint Laboratory of Collaborative Innovation for Environmental Quality, 511443 Guangzhou, China
[3]School of Environmental Science and Engineering, Qilu University of Technology (Shandong Academy of Sciences), 250353 Jinan, China
[4]State Key Laboratory of Organic Geochemistry and Guangdong Key Laboratory of Environmental Protection and Resources Utilization, Guangzhou Institute of Geochemistry, Chinese Academy of Sciences, 510640 Guangzhou, China
[5]State Joint Key Laboratory of Environmental Simulation and Pollution Control, College of Environmental Sciences and Engineering, Peking University, 100871 Beijing, China
[6]State Key Laboratory of Atmospheric Boundary Physics and Atmospheric Chemistry, Institute of Atmospheric Physics, Chinese Academy of Sciences, 100029 Beijing, China
[7]State Key Laboratory of Severe Weather & Key Laboratory for Atmospheric Chemistry of China Meteorology Administration, Chinese Academy of Meteorological Sciences, 100081 Beijing, China
[8]Multiphase Chemistry Department, Max Planck Institute for Chemistry, Mainz 55128, Germany

Correspondence: Bin Yuan (byuan@jnu.edu.cn) and Min Shao (mshao@pku.edu.cn)

Received: 17 February 2020 – Discussion started: 30 March 2020
Revised: 7 October 2020 – Accepted: 12 October 2020 – Published: 20 November 2020

Abstract. Higher alkanes are a major class of intermediate-volatility organic compounds (IVOCs), which have been proposed to be important precursors of secondary organic aerosols (SOA) in the atmosphere. Accurate estimation of SOA from higher alkanes and their oxidation processes in the atmosphere is limited, partially due to the difficulty of their measurement. High-time-resolution (10 s) measurements of higher alkanes were performed using NO^+ chemical ionization in proton transfer reaction time-of-flight mass spectrometry (NO^+ PTR-ToF-MS) at an urban site in Guangzhou in the Pearl River Delta (PRD) and at a rural site in the North China Plain (NCP). High concentrations were observed in both environments, with significant diurnal variations. At both sites, SOA production from higher alkanes is estimated from their photochemical losses and SOA yields. Higher alkanes account for significant fractions of SOA formation at the two sites, with average contributions of $7.0\,\% \pm 8.0\,\%$ in Guangzhou and $9.4\,\% \pm 9.1\,\%$ in NCP, which are comparable to or even higher than both single-ring aromatics and naphthalenes. The significant contributions of higher alkanes to SOA formation suggests that they should be explicitly included in current models for SOA formation. Our work also highlights the importance of NO^+ PTR-ToF-MS in measuring higher alkanes and quantifying their contributions to SOA formation.

Published by Copernicus Publications on behalf of the European Geosciences Union.

1 Introduction

As important components of fine particles, secondary organic aerosols (SOA) not only affect air quality and climate change but also threaten human health (An et al., 2019; Zhu et al., 2017; Chowdhury et al., 2018). Recent studies indicate large discrepancies between simulations and observations for SOA (de Gouw et al., 2008; Dzepina et al., 2009; Jiang et al., 2012), which are attributed to a limited understanding of complicated chemical and physical processes underlying SOA formation (Hallquist et al., 2009). A volatility basis set (VBS) model was developed to advance SOA modeling by improving the modeling of further multigenerational oxidation processes and incorporating numerous, yet unidentified, low-volatility precursors of SOA (Donahue et al., 2006), which substantially improved the agreement between SOA simulations and observations (Hodzic et al., 2010). However, there are still large uncertainties in current VBS models, including rate constants of oxidation reactions, the change of the O/C ratio in oxidation, and the relative importance of functionalization and fragmentation (Ma et al., 2017; Hayes et al., 2015). Explicit consideration of individual or a group of important semi-volatile organic compounds (SVOCs) or intermediate-volatility organic compounds (IVOCs) in the SOA model is urgently needed.

Higher alkanes as a major class of IVOCs (roughly corresponding to alkanes with 12–20 carbons) have been proposed as important SOA contributors in urban areas (Robinson et al., 2007; Yuan et al., 2013; Zhao et al., 2014). In typical urban areas, higher alkanes are reported to be mainly from vehicle emissions including diesel exhaust (Zhao et al., 2015) and gasoline exhaust (Zhao et al., 2016), corresponding generally to $\sim 4\,\%$ of nonmethane hydrocarbon (NMHC) emissions from on-road vehicles. Higher alkanes are estimated to produce as much SOA as, or even more SOA than, single-ring aromatics and polycyclic aromatic hydrocarbons from the oxidation of vehicle emissions, based on the chemical compositions measurements of vehicle exhaust (Zhao et al., 2015, 2016). Based on vehicle exhaust tests, higher alkanes were found to contribute $\sim 37\,\%$ to diesel-exhaust-derived SOA and $\sim 0.8\,\%$ to gasoline-exhaust-derived SOA (Gentner et al., 2012). Previous model studies have suggested that SOA simulation can be significantly improved when higher alkanes are considered in the model (Pye and Pouliot, 2012; Jathar et al., 2014; Wu et al., 2019). Although the concentrations of higher alkanes might be lower than other volatile organic carbon (VOC) classes (e.g., aromatics) in the atmosphere, higher alkanes are found to have much higher SOA yields, and the yields increase steadily with carbon number (Lim and Ziemann, 2005, 2009; Presto et al., 2010). For a given carbon number, SOA yields of higher alkanes reduce with branching of the carbon chain, especially under high-NO_x conditions (Lim and Ziemann, 2009; Tkacik et al., 2012; Loza et al., 2014).

Higher alkanes have been mainly measured using gas chromatography (GC)-based techniques, focusing on the compositions (Gong et al., 2011; Caumo et al., 2018), atmospheric concentration levels (Bi et al., 2003; Anh et al., 2018), and gas-particle partitioning (Xie et al., 2014; Sangiorgi et al., 2014). While most previous studies collected offline samples (usually 0.5 d–1 week) for GC-based analysis in the laboratory, hourly online measurements of *n*-alkanes using GC-based thermal desorption aerosol gas chromatography for semi-volatile organic compounds was recently developed and applied in ambient air (Zhao et al., 2013). Proton-transfer-reaction mass spectrometry (PTR-MS) using H_3O^+ as reagent ions is capable of measurements for many organic compounds with high time response and sensitivity (de Gouw and Warneke, 2007; Jordan et al., 2009; Yuan et al., 2017). Although H_3O^+ PTR-MS is responsive to large alkanes (> C8), these alkanes usually fragment into small masses with mass spectra difficult to interpret (Jobson et al., 2005; Gueneron et al., 2015). Recently, PTR-MS using NO^+ as reagent ions was demonstrated to provide fast online measurement of higher alkanes (Koss et al., 2016; Inomata et al., 2013). The high-time-resolution measurements of higher alkanes provide valuable information for SOA estimation, as the dependence of SOA yields on organic aerosol concentrations and other environmental parameters (e.g., temperature) (Lim and Ziemann, 2009; Presto et al., 2010; Loza et al., 2014; Lamkaddam et al., 2017) can be taken into account in more detail.

In this study, we utilize NO^+ chemical ionization in proton transfer reaction time-of-flight mass spectrometry (hereafter referred to as NO^+ PTR-ToF-MS) to measure higher alkanes at two different sites in China, one urban site in the Pearl River Delta (PRD) region and one rural site in the North China Plain (NCP) region. We use the datasets along with measurements of other pollutants to estimate contributions to SOA formation from higher alkanes and other SOA precursors. The observation-constrained SOA formation of this study is a step forward from previous modeling studies, which proposed the important roles of SVOCs and IVOCs (Jiang et al., 2012; Yang et al., 2018; Wu et al., 2019) including higher alkanes (Yuan et al., 2013) in SOA formation in China.

2 Methods

Field campaigns were conducted at an urban site in Guangzhou in the PRD region during September–November 2018 and at a rural site in Baoding in NCP during November–December 2018. A detailed description of the measurement sites can be found in the Supplement (Fig. S1).

2.1 NO^+ PTR-ToF-MS measurements

PTR-MS is a technique that allows for fast and sensitive measurements of VOCs at trace levels in the air. PTR-MS using H_3O^+ chemistry has been demonstrated to measure alkenes, aromatics, and even oxygenated VOCs (Yuan et al., 2017; Wu et al., 2020). Here, PTR-MS with NO^+ chemistry was used to detect higher alkanes, through hydride abstraction by NO^+ forming mass ($m-1$, where m is the molecular mass) ions (Koss et al., 2016; Inomata et al., 2013).

A commercially available PTR-ToF-MS instrument (Ionicon Analytik, Austria) with a mass resolving power of 4000 m Δm^{-1} was used for this work. To generate NO^+ as reagent ions, ultra-high-purity air (5.0 sccm) was directed into the hollow cathode discharge ion source. The pressure of the drift tube was maintained at 3.8 mbar. Voltages of ion source and drift chamber were explored (Fig. S2) in the laboratory to optimize the generation of NO^+ ions relative to H_3O^+, O_2^+, and NO_2^+ and minimize alkane fragmentation. The intensities of primary ion NO^+ and impurities (O_2^+, H_3O^+, and NO_2^+) and the ratio of O_2^+ to NO^+ during two campaigns are shown in Figs. S3 and S4, respectively. The ratio of O_2^+/NO^+ (Fig. S4a) is basically stable at 2–4 % during the PRD campaign except during 26 October–2 November 2018 (7–10 %). For the NCP campaign, the ratio of O_2^+/NO^+ (Fig. S4b) fluctuates between 10 and 40 % in the early stage of the campaign and remains stable at ~20 % in the later stage of the campaign. Such fluctuations are attributed to the humidity effect in the ambient air (Fig. S5). Ion source voltages of U_s and U_{so} were selected as 40 and 100 V, while U_{drift} and U_{dx} were set to 470 and 23.5 V, resulting in an E/N (electric potential intensity relative to gas number density) of 60 Td. NO^+ PTR-ToF-MS data were analyzed using Tofware software (Tofwerk AG) for high-resolution peak fitting. A description of the algorithm can be found in Stark et al. (2015) and Timonen et al. (2016). Figure 1 shows the high-resolution peak fitting to the averaged mass spectra on a typical day (12 October 2018) for m/z 169, m/z 211, and m/z 281, at which masses produced by dodecane ($C_{12}H_{25}^+$), pentadecane ($C_{15}H_{31}^+$), and eicosane ($C_{20}H_{41}^+$) are detected. It is observed that the ions from higher alkanes lie at the rightmost position at each nominal mass, with signals being either the largest or among the largest ions at these nominal masses, which help to achieve high precision for determined signals of higher alkanes from high-resolution peak fitting (Cubison and Jimenez, 2015; Corbin et al., 2015).

In this study, we normalize the raw ion count rate of higher alkanes to the primary ion (NO^+) at a level of 10^6 cps to account for fluctuations of ion source and detector. Calibrations were conducted every 1–2 d under both dry conditions (relative humidity < 1 %) and ambient humidity conditions using a gas standard with a series of n-alkanes (Apel Riemer Environmental Inc.) during the NCP campaign (Fig. 2a). Sensitivities of n-alkane (C8–C15) standards were obtained during the campaign (Fig. S6), which are defined as the normalized

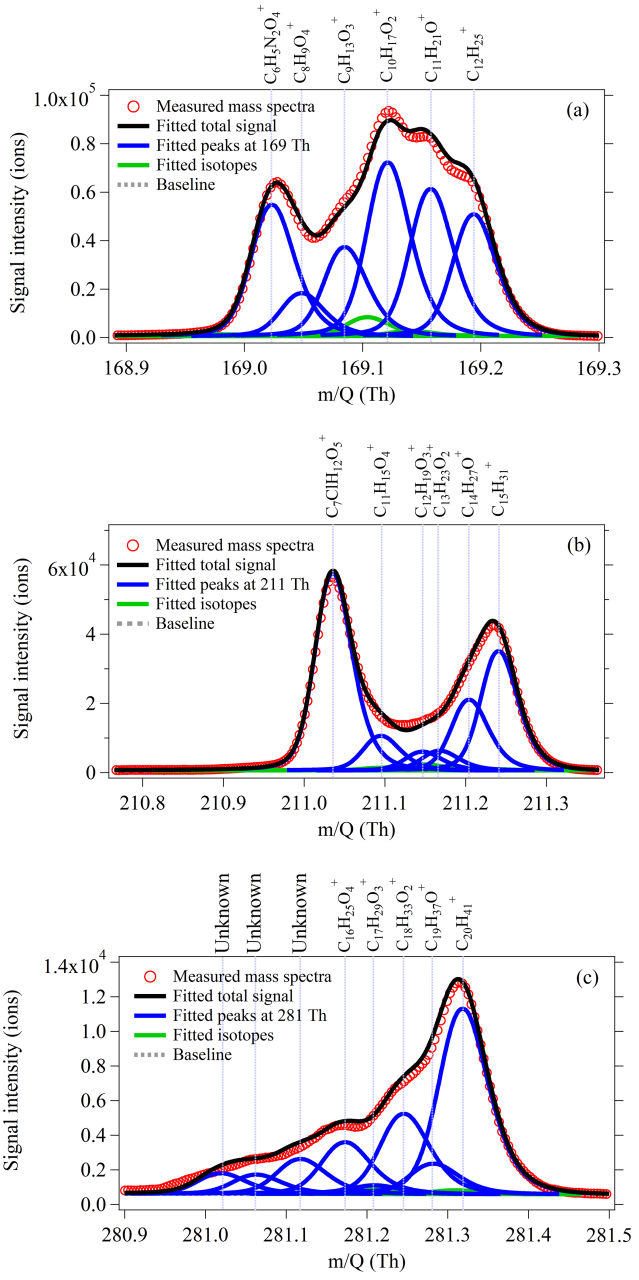

Figure 1. High-resolution (HR) peak fitting to the averaged mass spectra on a typical day (12 October 2018) for m/z 169 **(a)**, m/z 211 **(b)**, and m/z 281 **(c)**, at which masses produced by dodecane ($C_{12}H_{25}^+$), pentadecane ($C_{15}H_{31}^+$), and eicosane ($C_{20}H_{41}^+$) are detected using NO^+ PTR-ToF-MS.

signal of hydride abstraction ions for each higher alkane at 1 ppbv in units of normalized counts per second per parts per billion (ncps ppb^{-1}). The fluctuations of sensitivities during the NCP campaign may be influenced by the variations of O_2^+ signals (Fig. 2), because the reactions of O_2^+ with alkanes can be proceeded by both charge transfer and hydride abstraction (Amador et al., 2016), which may affect the ion

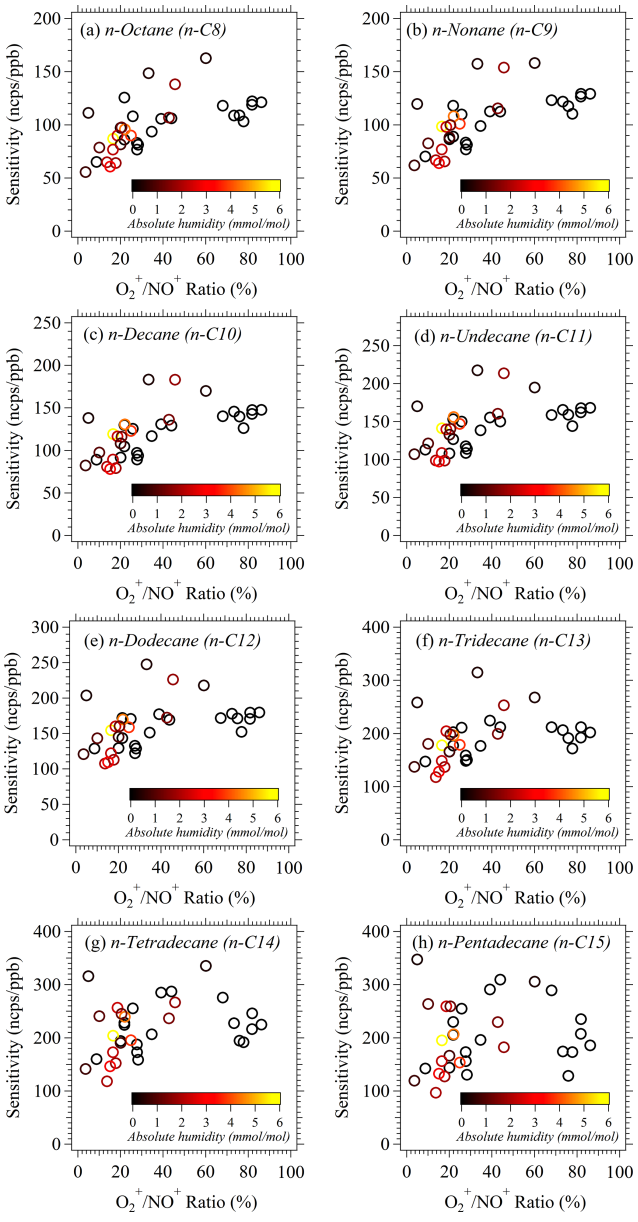

Figure 2. The relationship of sensitivities of n-alkanes (C8–C15) vs. O_2^+/NO^+ ratios during the NCP campaign. The data points are color-coded using absolute humidity during the calibration.

signals of alkanes with NO^+ reactions. Therefore, we use the daily ambient calibration results to quantify the concentration of higher alkanes during the NCP campaign to reflect the variations of sensitivity from day to day. For the measurements without daily calibrations, we used closest calibration results according to corresponding ambient O_2^+/NO^+ ratios and ambient humidity. Since we got the alkane standard in a very late period of the PRD campaign, we did not have the daily calibrations for this campaign. Therefore, we use the sensitivity of each alkane under corresponding O_2^+/NO^+ conditions obtained from lab experiments after this campaign and also consider the humidity effects (Fig. 3b and c) to quantify the concentration of higher alkanes during the PRD campaign. Humidity-dependent behaviors of n-alkanes (C8–C15) were evaluated in the laboratory at different humidity levels (0–33 mmol mol^{-1}) by diluting a higher alkane standard into humidified air to reach an approximately 1 ppb mixing ratio. As shown in Figs. 3b and c and S7a, the normalized signal of all product ions ($m-1$) and the fragment ions of n-alkane (C8–C15) standards decrease with the increase of humidity. These decreasing patterns are probably due to the decreasing primary reagent ions (NO^+ and O_2^+) as the humidity increases (Fig. S7b). Thus, the humidity correction should be applied for the quantitation of higher alkanes using NO^+ PTR-ToF-MS.

The fragmentation patterns for selected n-alkanes and their branched isomers are measured with NO^+ PTR-ToF-MS by introducing commercially acquired pure chemicals (Fig. S8). Figure 4a shows the fractions of hydride abstraction $m-1$ ions in the mass spectra of C8–C20 n-alkanes in NO^+ PTR-ToF-MS. Generally, larger n-alkanes show a lower degree of fragmentation in the mass spectra with higher fractions contributed by $m-1$ ions. The fractions of $m-1$ ions account for more than 60 % of total ion signals for $>$C12 n-alkanes. We also observe good correlation between the fractions of $m-1$ ions in mass spectra and the determined sensitivities for C8–C15 n-alkanes. As C16–C21 n-alkanes exhibit similar degrees of fragmentation to C15, sensitivities of the alkanes were assumed to be same as that of C15 n-alkane (Fig. 4b). Comparison of the degree of fragmentation between n-alkanes and their branched isomers (Fig. S9) shows that the substituted groups have a small effect on the degrees of fragmentation for product ions, at least for branched isomers with up to four substituted methyl groups. Previous studies demonstrated that the branched alkanes from emissions of fossil-fuel-related sources are primarily with one or two alkyl branches (Chan et al., 2013; Isaacman et al., 2012). Therefore, we conclude that the branched isomers of higher alkanes should have similar response factors to their normal analogs. As a result, the concentration of higher alkanes from NO^+ PTR-ToF-MS should be regarded as the summed concentrations of n-alkanes and branched alkanes that have the same chemical formulas.

Detection limits are calculated as the concentrations at which signal counts are 3 times the SD of measured background counts (Bertram et al., 2011; Yuan et al., 2017). As shown in Table 1, detection limits are determined to be on the order of 0.7–1.3 ppt for higher alkanes for 1 min integration times. Delay time is calculated as the time it takes for the signal to drop to 10 % of its initial value caused by the step-function change in sample concentration (Pagonis et al., 2017). The delay times of higher alkanes for the field measurements in this study and some other measurements (e.g., emission source measurements and tubing loss test) in the laboratory are summarized in Fig. S10. It is found that de-

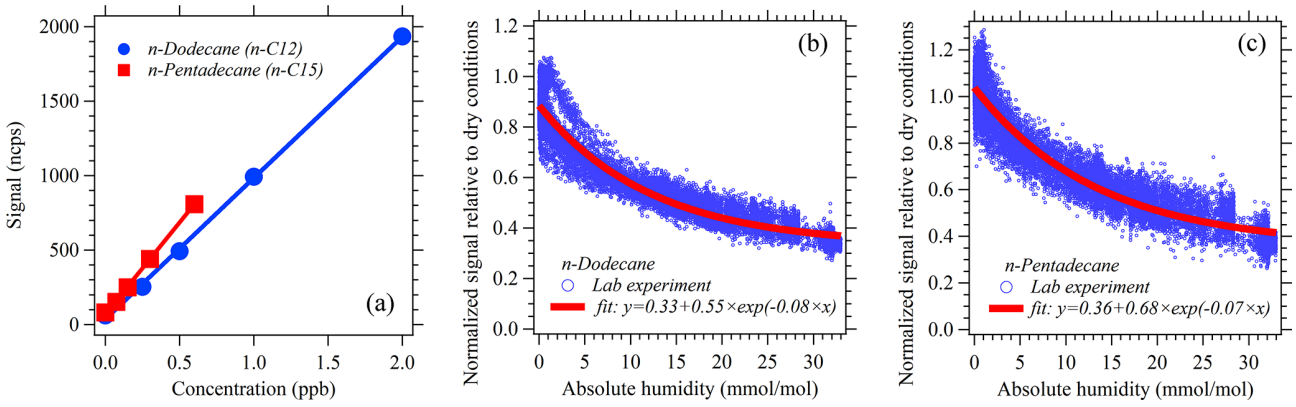

Figure 3. **(a)** Calibrations of *n*-dodecane and *n*-pentadecane under dry conditions. **(b)** Humidity dependence of *n*-dodecane. **(c)** Humidity dependence of *n*-pentadecane.

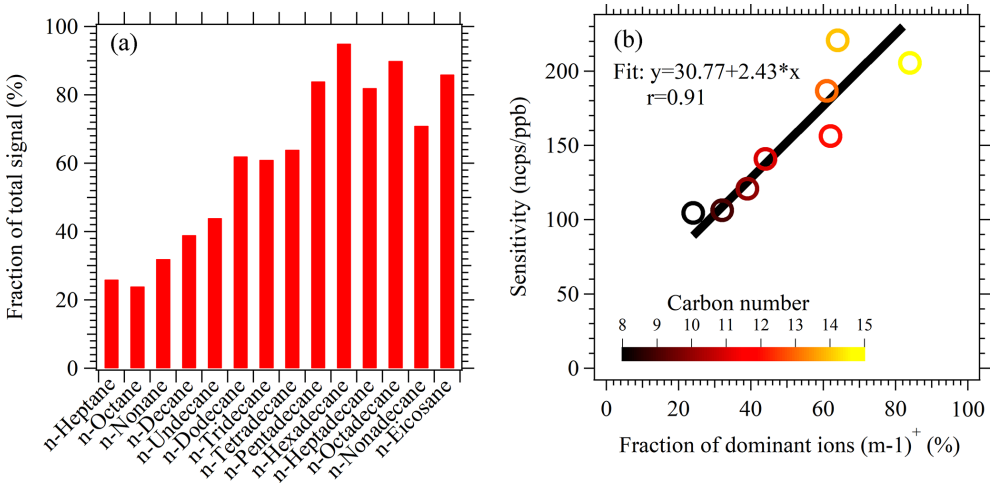

Figure 4. **(a)** The fractions of product ions ($m-1$) from hydride abstraction of C8–C20 *n*-alkanes in NO^+ PTR-ToF-MS. **(b)** Scatterplot of sensitivities under dry conditions vs. the fractions of hydride abstraction ions for C8–C15 *n*-alkanes.

lay times for various alkanes are in a range of a few seconds to few minutes, among which higher-volatility alkanes (C8–C15) are better than 1 min and lower-volatility alkanes (C16–C21) are relatively long, reaching several minutes. These results suggest that alkanes with a higher carbon number, especially C20 and C21. might be influenced by the tubing delay effect during the measurements. However, as shown later in Sect. 3.1, the lower-volatility alkanes exhibit very similar diurnal variations to higher-volatility alkanes during both campaigns in PRD and NCP, implying that the tubing effects should not significantly affect temporal variations of higher alkanes reported in this study.

During these two campaigns, PTR-ToF-MS automatically switches between H_3O^+ and NO^+ chemistry every 10–20 min with a 10 s measurement resolution. Switching between H_3O^+ and NO^+ ion modes is provided by the PTR-MS Manager (v3.5) software developed by Ionicon Analytik (Table S1 in the Supplement). Drift chamber pressure is held constant at 3.8 mbar in both modes during the campaigns (Fig. S11a). It usually takes < 10 s for H_3O^+ ions and ~ 60 s for NO^+ ions to re-stabilize after automatically switching between the two measurement modes (Fig. S11b). The ambient measurement data from the transition period (~ 1 min) were discarded. Ambient air was continuously introduced into PTR-ToF-MS through Teflon tubing (1/4 in.) with an external pump at 5.0 L min^{-1}, with tubing length of ~ 8 and ~ 3 m during the PRD and the NCP campaign, respectively. The inlet tubing was heated all the way to the sampling inlet to avoid water vapor condensation by an insulating tube with a self-controlled heater wire (40 °C) wrapping outside. The calculated residence time for the inlet was ~ 3 s for the PRD campaign and ~ 1 s for the NCP campaign. The tubing loss experiments were conducted in the laboratory by introducing standards of higher alkanes (*n*-C8–C15), monoaromatics (benzene, toluene, *o*-xylene, and 1,2,4-trimethylbenzene), isoprenoids (isoprene and α-pinene), and naphthalene into

Table 1. Fractions of product ions ($m-1$) in mass spectra, and sensitivities and detection limits of higher alkanes in NO^+ PTR-ToF-MS.

Compounds	Ions	Fractions of ($m-1$) ions (%)	Sensitivities (ncps ppb^{-1})	Detection limit for 10 s integration (ppt)	Detection limit for 1 min integration (ppt)
n-Octane	$C_8H_{17}^+$	24	104.6	3.5	1.3
n-Nonane	$C_9H_{19}^+$	32	106.3	3.2	1.2
n-Decane	$C_{10}H_{21}^+$	39	120.9	3.5	1.3
n-Undecane	$C_{11}H_{23}^+$	44	140.9	3.3	1.2
n-Dodecane	$C_{12}H_{25}^+$	62	156.3	2.4	0.9
n-Tridecane	$C_{13}H_{27}^+$	61	186.6	2.1	0.8
n-Tetradecane	$C_{14}H_{29}^+$	64	220.7	1.9	0.7
n-Pentadecane	$C_{15}H_{31}^+$	84	205.5	1.7	0.6
n-Hexadecane	$C_{16}H_{33}^+$	95	–	1.6	0.6
n-Heptadecane	$C_{17}H_{35}^+$	82	–	1.8	0.7
n-Octadecane	$C_{18}H_{37}^+$	90	–	1.8	0.7
n-Nonadecane	$C_{19}H_{39}^+$	71	–	1.2	0.4
n-Eicosane	$C_{20}H_{41}^+$	86	–	1.9	0.7
n-Heneicosane	$C_{21}H_{43}^+$	–	–	2.0	0.7

PTR-ToF-MS through 8 m of Teflon tubing (1/4 in.) at room temperature with an external pump at 5.0 L min^{-1} (Fig. S12). The tubing loss of these compounds is found to be $< 5\,\%$ except for *n*-C15 ($\sim 8\,\%$) and naphthalene ($\sim 10\,\%$). Background measurement of 3 min was conducted in each cycle of NO^+ and H_3O^+ measurements by introducing the ambient air into a catalytic converter at a temperature of 367 °C.

2.2 Other measurements

During the Guangzhou campaign, an online GC-MS/FID (flame ionization detector) system was used to measure C2–C11 *n*-alkanes, alkenes, and aromatics with a time resolution of 1 h (Yuan et al., 2012). Non-refractory components in particulate matter with a diameter less than 1 µm (PM_1) – including nitrate, sulfate, ammonium, chloride, and organics – were measured with an Aerodyne high-resolution time-of-flight aerosol mass spectrometer (HR-ToF-AMS) and a time-of-flight aerosol chemical speciation monitor (ToF-ACSM) in PRD and NCP, respectively. Trace gaseous species (CO, NO, NO_2, O_3, and SO_2) were measured using commercial gas analyzers (Thermo Scientific). Photolysis frequencies were measured using a spectroradiometer (PFS-100, Focused Photonics Inc.). In addition, temperature, pressure, relative humidity, and wind were continuously measured during two campaigns.

3 Results and discussion

3.1 Ambient concentrations and diurnal variations of higher alkanes

Although NO^+ chemistry has been shown to be valuable in measuring many organic species, the applications in real atmosphere of different environments are still rare (Koss et al., 2016). Here, we compared the measurements of various VOCs from NO^+ PTR-ToF-MS with both H_3O^+ PTR-ToF-MS and GC-MS/FID during the two campaigns. Overall, good agreement between PTR-ToF-MS (both H_3O^+ and NO^+ chemistry) and GC-MS/FID was obtained for aromatics and oxygenated VOCs except benzene (Figs. S13 and S14). Benzene measurements in H_3O^+ chemistry show a large difference from benzene measured with NO^+ chemistry in the earlier period of the PRD campaign (11 September–14 October 2018), but good agreement was obtained for the rest of the measurement period. Considering the good agreement of benzene between NO^+ PTR-ToF-MS and GC-MS/FID, we used benzene data from NO^+ measurement in this study. The time series and diurnal variations of alkanes (C8–C11) between NO^+ PTR-ToF-MS and GC-MS/FID are shown in Fig. 5 (and Fig. S15). Similar temporal trends for these alkanes are observed with the two instruments. However, the diurnal patterns of total alkanes from NO^+ PTR-ToF-MS have a deeper afternoon trough than the *n*-alkanes measured using GC-MS, implying that *n*-alkanes

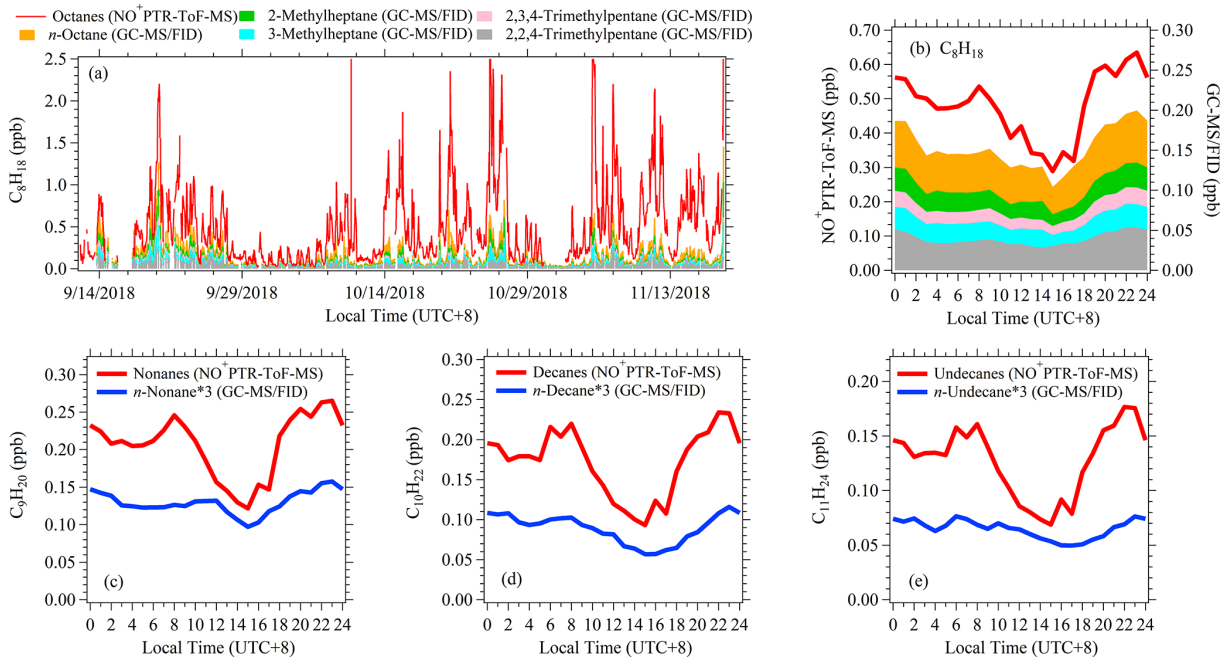

Figure 5. Comparisons of times series and diurnal variations of alkanes measured using NO^+ PTR-ToF-MS and GC-MS/FID in PRD. **(a)** Time series of C8 alkanes measured using NO^+ PTR-ToF-MS, and C8 *n*-alkane and four branched isomers measured using GC-MS/FID. **(b)** Diurnal variations of C8 alkanes. **(c–e)** Diurnal variations of C9–C11 alkanes measured using NO^+ PTR-ToF-MS and C9–C11 *n*-alkanes measured using GC-MS/FID.

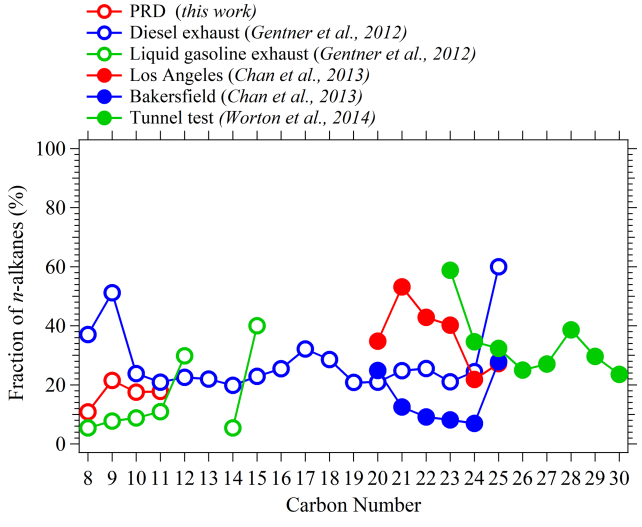

Figure 6. Fractions of *n*-alkanes in higher alkanes with the same formulas in gas phase (hollow dots) and particle phase (solid dots) derived from this study, ambient air in Los Angeles and Bakersfield, Caldecott Tunnel, and vehicle exhaust (Chan et al., 2013; Gentner et al., 2012; Worton et al., 2014).

may have different temporal variations compared with those of total alkanes. The concentrations at each carbon number from NO^+ PTR-ToF-MS are ∼3–6 times those from GC-MS/FID. This is expected, as dozens to hundreds of isomers exist for alkanes with carbon numbers in this range (Goldstein and Galbally, 2007), and GC-MS/FID only measured one or a few isomers. Based on measurements from NO^+ PTR-ToF-MS and GC-MS/FID, we computed the molar concentration fractions of *n*-alkanes for each carbon number (Fig. 6 and Table S1). We found the fractions are in the range of 11–21 % for a carbon number of 8–11, which are comparable with results of ambient air in California, a tunnel test, and vehicle exhaust (Fig. 6 and Table S2) (Chan et al., 2013; Worton et al., 2014; Gentner et al., 2012). These results indicate the importance of branched alkanes in concentrations of higher alkanes and their potential contributions to SOA formation. It also has strong implications for the merits of NO^+ PTR-ToF-MS in measuring the sum of the alkanes with the same formula for estimation of SOA contributions, as discussed later.

Table 2 summarizes means and SDs of concentrations of higher alkanes (C8–C21) measured in PRD and in NCP. The mean concentrations of *n*-alkanes measured at a suburban site in Paris, France (Ait-Helal et al., 2014), and an urban site in Pasadena, USA, are also included in Table 1 for comparison. According to the fraction of *n*-alkanes, the mean concentrations of *n*-alkanes in China are found to be comparable to those from Paris and higher than in Pasadena. In

Table 2. Mean concentrations of alkanes (C8–C21) in different sites worldwide.

Compounds	Formula	PRD, China[a] Alkanes (ppt)	PRD, China[b] *n*-Alkanes (ppt)	NCP, China[a] Alkanes (ppt)	Paris, France[c] *n*-Alkanes (ppt)	Pasadena, USA[d] Alkanes (ppt)
Octane	C_8H_{18}	482 ± 488	50 ± 49	412 ± 270	–	–
Nonane	C_9H_{20}	208 ± 186	43 ± 32	252 ± 162	14 ± 13	–
Decane	$C_{10}H_{22}$	174 ± 199	29 ± 28	224 ± 147	24 ± 22	–
Undecane	$C_{11}H_{24}$	129 ± 138	21 ± 17	170 ± 119	19 ± 16	–
Dodecane	$C_{12}H_{26}$	122 ± 120	–	129 ± 86	22 ± 21	8 ± 1
Tridecane	$C_{13}H_{28}$	66 ± 60	–	89 ± 59	13 ± 12	6 ± 1
Tetradecane	$C_{14}H_{30}$	50 ± 47	–	57 ± 39	27 ± 23	9 ± 2
Pentadecane	$C_{15}H_{32}$	45 ± 42	–	46 ± 33	23 ± 18	5 ± 0.8
Hexadecane	$C_{16}H_{34}$	36 ± 33	–	32 ± 24	22 ± 19	4 ± 1
Heptadecane	$C_{17}H_{36}$	21 ± 20	–	18 ± 14	–	3 ± 0.4
Octadecane	$C_{18}H_{38}$	13 ± 14	–	11 ± 9	–	1.6 ± 0.5
Nonadecane	$C_{19}H_{40}$	5 ± 9	–	4 ± 7	–	0.7 ± 0.2
Eicosane	$C_{20}H_{42}$	0.7 ± 4	–	3 ± 6	–	0.24 ± 0.08
Heneicosane	$C_{21}H_{44}$	0.5 ± 5	–	2 ± 5	–	0.15 ± 0.1

[a] Alkanes measured with NO^+ PTR-ToF-MS. [b] *n*-Alkanes measured with GC-MS. [c] *n*-Alkanes from Ait-Helal et al. (2014). [d] *n*-Alkanes from Zhao et al. (2014).

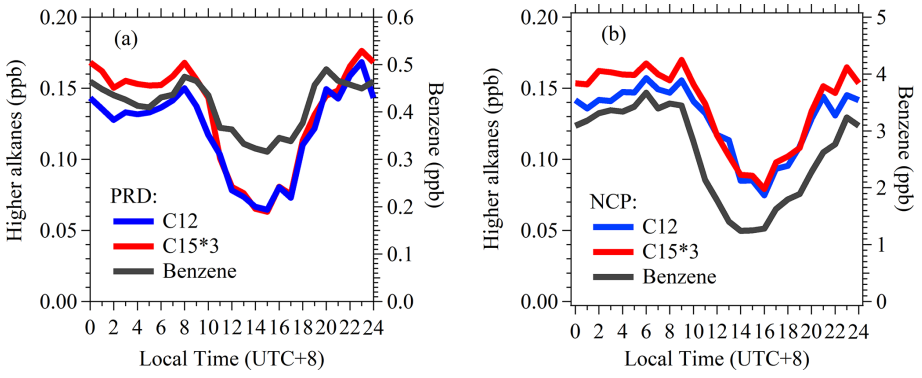

Figure 7. Diurnal variations of C12 alkanes, C15 alkanes, and benzene in PRD **(a)** and NCP **(b)**.

general, concentrations of higher alkanes concentration decrease with the increase of carbon number, with octanes (C8) at ~0.5 ppb and heneicosanes (C21) at ~0.002 ppb. This decreasing pattern of carbon distribution is the result of lower emissions from sources (Gentner et al., 2012), larger reactivity towards OH radicals (Atkinson et al., 2008; Keyte et al., 2013), and larger fractions partitioning to particles (Liang et al., 1997; Xie et al., 2014; Zhao et al., 2013) in the atmosphere.

The diurnal variations of selected higher alkanes are shown in Fig. 7. C12 alkanes and C15 alkanes exhibit similarly strong diurnal variations at both sites, with relatively high levels at night and minimum concentrations detected in the late afternoon at both sites. Such diurnal patterns are consistent with other primary VOC species (e.g., aromatics). In PRD, the diurnal variations of higher alkanes were the result of faster chemical removal in the daytime and shallow boundary layer heights at night. Since OH concentrations in NCP during winter were much lower than in PRD during autumn (Fig. S16), diurnal variations of higher alkanes in NCP were mainly influenced by the change of boundary layer. The diurnal profiles of other higher alkanes are similar to C12 and C15 alkanes (Fig. S17).

3.2 Estimation of the contributions of higher alkanes to SOA formation

A time-resolved approach based on consideration of photooxidation processes with the OH radical (Ait-Helal et al., 2014) was applied to estimate contributions of higher alkanes to SOA during these two campaigns. In order to evaluate the relative importance to SOA of different precursors, the same method was also used for monoaromatics, naphthalenes, and isoprenoids.

This method considers the amount of chemical removal based on the parameterized photochemical age, which was

widely used to quantify contributions of different VOC precursors to SOA formation (Zhao et al., 2014; Ait-Helal et al., 2014; de Gouw et al., 2009). The contributions to SOA formation from different compounds are determined by the ratios of calculated SOA production amounts from individual precursors (Supplement, Appendix 2) and SOA concentrations derived from factor analysis of OA measurements by AMS (Supplement, Appendix 3). In this method, SOA formation for a given compound can be estimated by

$$[\mathrm{SOA}_i]_t = [\mathrm{VOC}_i]_t \cdot (e^{k_{\mathrm{VOC}_i} \cdot ([\mathrm{OH}] \cdot \Delta t)} - 1) \cdot \mathrm{yield}_i, \quad (1)$$

where $[\mathrm{SOA}_i]_t$ is the calculated SOA production ($\mu g\,m^{-3}$) for a given specific compound VOC_i at time t, $[\mathrm{VOC}_i]_t$ is the VOC_i concentration measured at time t ($\mu g\,m^{-3}$), yield_i is the SOA yield data summarized from chamber studies, and k_{VOC_i} is the rate constant of VOC_i with the OH radical ($cm^3\,molecule^{-1}\,s^{-1}$). [OH] is the OH concentration ($molecules\,cm^{-3}$); Δt is the photochemical age. In this study, we calculated the [OH] $\times\ \Delta t$ ($molecules\,cm^{-3}\,s$), which was considered as OH exposure in some studies (Jimenez et al., 2009). The OH exposure is estimated by the ratio of $m + p$-xylene to ethylbenzene with different reactivity for anthropogenic VOCs and by the oxidation processes of isoprene for biogenic VOCs (Apel et al., 2002; Roberts et al., 2006) (see details in the Supplement, Appendix 4, and Fig. S18). Since biogenic emissions were pretty weak during the cold winter (mean temperature: $0.5 \pm 3.6\,^{\circ}C$) during the NCP campaign, measured concentrations of isoprene and monoterpenes are regarded as being of anthropogenic origin during the winter campaign in NCP, especially given the fact that they showed similar variations, diurnal profiles, and strong correlation with CO and anthropogenic VOC species (Fig. S19). A previous study in Helsinki also found the importance of anthropogenic emission in monoterpene concentrations (Hellén et al., 2012).

Based on Eq. (1), SOA production from higher alkanes (C8–C21 alkanes), monoaromatics (benzene, toluene, C8 aromatics, C9 aromatics, and styrene), naphthalenes (naphthalene, methylnaphthalenes, and dimethylnaphthalenes), and isoprenoids (isoprene and monoterpenes) was calculated. The concentration data of higher alkanes, isoprenoids, and benzene were taken from measurements using NO^+ PTR-ToF-MS. The concentration data of naphthalenes (Fig. S20) and monoaromatics except benzene were taken from measurements using H_3O^+ PTR-ToF-MS. Details about the H_3O^+ PTR-ToF-MS measurements can be found in Wu et al. (2020). The OH reaction rate constant of each compound was taken from the literature (Atkinson, 2003). SOA yield data used here for higher alkanes (Lim and Ziemann, 2009; Presto et al., 2010; Loza et al., 2014; Lamkaddam et al., 2017), monoaromatics (Li et al., 2016; Ng et al., 2007; Tajuelo et al., 2019), naphthalenes (Chan et al., 2009), and isoprenoids (Ahlberg et al., 2017; Carlton et al., 2009; Edney et al., 2005; Kleindienst et al., 2006; Pandis et al., 1991) were summarized from reported values in the literature, with the consideration of the influence of organic aerosol concentration (Fig. S21) to SOA yields (Donahue et al., 2006) (Figs. S22 and 23). SOA yields under high-NO_x conditions are used in this study, as relatively high NO_x concentrations in PRD (42.6 ± 33.7 ppb) and in NCP (81.7 ± 57.0 ppb) (Fig. S24) would cause RO_2 radicals from organic compounds mainly reacting with NO (Bahreini et al., 2009).

Both OH reaction rate constants and SOA yields of n-alkanes reported in the literature are applied for higher alkanes, as most of the chamber studies have focused on n-alkanes. Considering that the SOA yields of branched alkanes are lower than those of n-alkanes, which is dependent on chemical structures of the carbon backbone (Lim and Ziemann, 2009; Tkacik et al., 2012; Loza et al., 2014), the estimation of SOA from alkanes in this study might be a little overestimated. As shown above, temperature (mean temperature: $0.5 \pm 3.6\,^{\circ}C$) in the NCP winter campaign was significantly lower than the temperature (usually $25\,^{\circ}C$) at which SOA yields are derived from chamber studies. Temperature can significantly influence SOA yields, with higher yields at lower temperature (Takekawa et al., 2003; Lamkaddam et al., 2017). It might cause underestimation of SOA production from various precursors in winter in NCP.

The calculated results of SOA production for different higher alkanes are shown in Fig. 8. Although lower concentrations of heavier alkanes were observed for both campaigns, the calculated SOA production is largest for C12–C18 (Fig. 8b). This is for two reasons: (1) alkanes with a larger carbon number have larger SOA yields. The calculated average SOA yields (Table S3) during the two campaigns are both larger than 0.2 for $>$C12 alkanes and increase to near unity for C20–C21 alkanes. (2) Larger alkanes are relatively more reactive than lighter ones, which results in larger proportions of calculated concentrations that have been chemically consumed in the atmosphere (the concentrations labeled "consumed" in Fig. 8a). The distribution of contributions from alkanes with a different carbon number to SOA formation shown here is in good agreement with previous results from volatility calculation for precursors (de Gouw et al., 2011; Liggio et al., 2016). The peaks in alkane SOA production occur around C15 in both the PRD and NCP campaigns, which is a great result that shows the importance of IVOCs for SOA.

Along with higher alkanes, SOA production for monoaromatics, naphthalenes, and isoprenoids is shown in Fig. 9 (and Figs. S25–S27). Compared to monoaromatics, higher alkanes are associated with lower concentrations (Fig. S28). However, higher alkanes play an important role in SOA formation due to their high SOA yields (Fig. S29). The total average SOA production from C8–C21 alkanes is 0.6 ± 0.8 and $0.7 \pm 0.8\,\mu g\,m^{-3}$ in PRD and NCP, respectively. The SOA formed from higher alkanes account for $7.0\,\% \pm 8.0\,\%$ and $9.4\,\% \pm 9.1\,\%$ of SOA formation in PRD and NCP, respectively. The contributions of monoaromatics to SOA for-

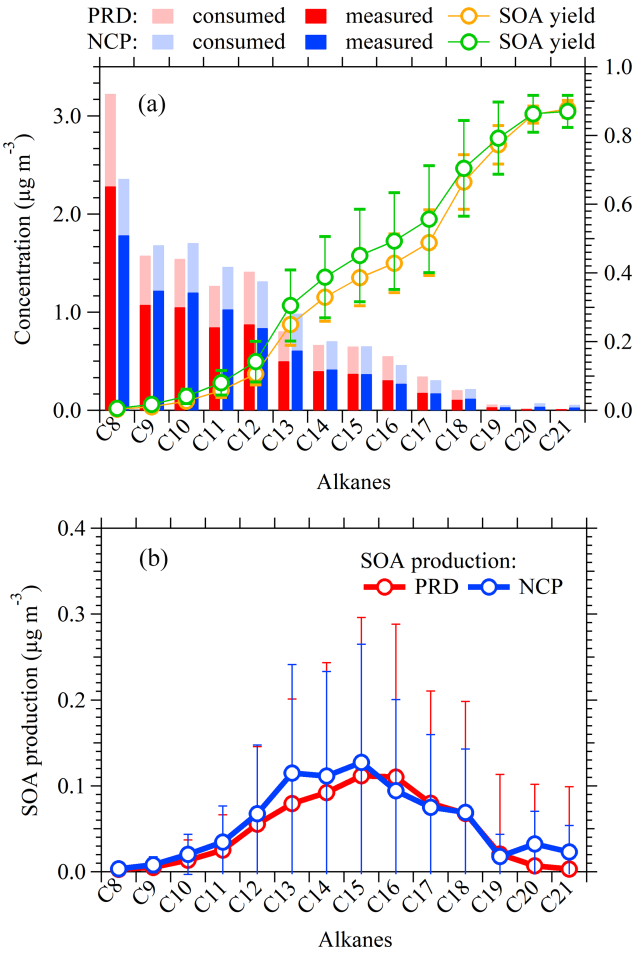

Figure 8. **(a)** Concentrations measured using NO^+ PTR-ToF-MS, calculated consumed concentrations, and average SOA yields for C8–C21 alkanes in PRD and NCP. The consumed concentrations represent the chemical losses of higher alkanes, which are calculated by dividing the estimated SOA from each alkane by the corresponding SOA yields. The error bars represent SDs (1δ) over the averaging period of calculated SOA yields. **(b)** Calculated average SOA productions for C8–C21 alkanes in PRD and NCP. The error bars represent SDs (1δ) over the averaging period of calculated SOA production.

mation are $6.2\,\% \pm 7.7\,\%$ and $9.4\,\% \pm 17.4\,\%$ in PRD and NCP, respectively. Naphthalenes have been proposed to be important precursors of SOA from laboratory chamber studies (Kleindienst et al., 2012). In this study, we determine that $2.8\,\% \pm 4.6\,\%$ of SOA in PRD and $11.1\,\% \pm 14.3\,\%$ of SOA in NCP are contributed by naphthalenes. The SOA contribution from naphthalenes determined for NCP is comparable to the results ($10.2\,\% \pm 1.0\,\%$) obtained during haze events in Beijing in a recent study (Huang et al., 2019). Significant contribution from monoterpenes to SOA ($8.7\,\% \pm 14.6\,\%$) is observed in NCP. As mentioned above, we attribute these isoprene and monoterpenes to anthropogenic emissions in this region. The SOA precursors considered in this study in total could explain 14.9–29.0 % and 16.4–125.3 % of SOA formation in PRD and NCP, respectively. The influence of chamber-based vapor wall losses on SOA yields was examined in previous studies (Zhang et al., 2014), and the results show that the literature-reported SOA yields are low by factors of $\sim$1.1–2.2 for the high-NO_x conditions (Table S4). This suggests that the SOA estimations in this study might be correspondingly underestimated. The low explained percentages of SOA formations in both PRD and NCP (Fig. 9c and d) imply that some other SOA precursors (e.g., alkylcyclohexanes, alkylbenzenes, and cyclic and polycyclic aliphatic materials) (Zhao et al., 2015; Drozd et al., 2019) or formation pathways (e.g., aqueous reactions) (Kuang et al., 2020) are contributing significantly to SOA formation. Compared to a previous study in northern China (Yuan et al., 2013), the missing gap of SOA formation declined after explicitly considering higher alkanes and naphthalenes in SOA production.

As shown in Fig. 9, we find that higher alkanes (C8–C21) contribute significantly to SOA formation at both an urban site in autumn in PRD and a rural site in winter in NCP. The contributions from higher alkanes are either comparable to or higher than both monoaromatics and naphthalenes. Another estimation method considering instantaneous SOA production rates obtained similar results (Fig. S30), which confirms the results from the photochemical age based on the parameterization method shown above. The importance of higher alkanes in SOA formation has also been proposed in several previous SOA modeling studies (Pye and Pouliot, 2012; Zhao et al., 2014). These results, along with our results from observations in ambient atmosphere, underline that the inclusion of higher alkanes in SOA models in the atmosphere should be considered if possible.

4 Conclusions

In this study, we utilized a NO^+ PTR-ToF-MS to measure C8–C21 alkanes in two different environments in China. Based on a series of laboratory experiments, we show that NO^+ PTR-ToF-MS can provide online measurements of higher alkanes with high accuracy and fast response. The measured concentrations of higher alkanes were relatively high during the two campaigns. The diurnal profiles of higher alkanes are similar to anthropogenic VOCs, implying they are emitted from anthropogenic sources.

On the basis of measurements of higher alkanes using NO^+ PTR-ToF-MS, we successfully take into account their contributions to SOA formation. The time-resolved measurements of higher alkanes using NO^+ PTR-ToF-MS provide the opportunity to accurately apply the photochemical-age-based parameterization method. As there is no separation before detection in PTR-ToF-MS, the measured concentrations of NO^+ PTR-ToF-MS represent all of the compounds that contribute to the product ions ($m-1$ ions), which include

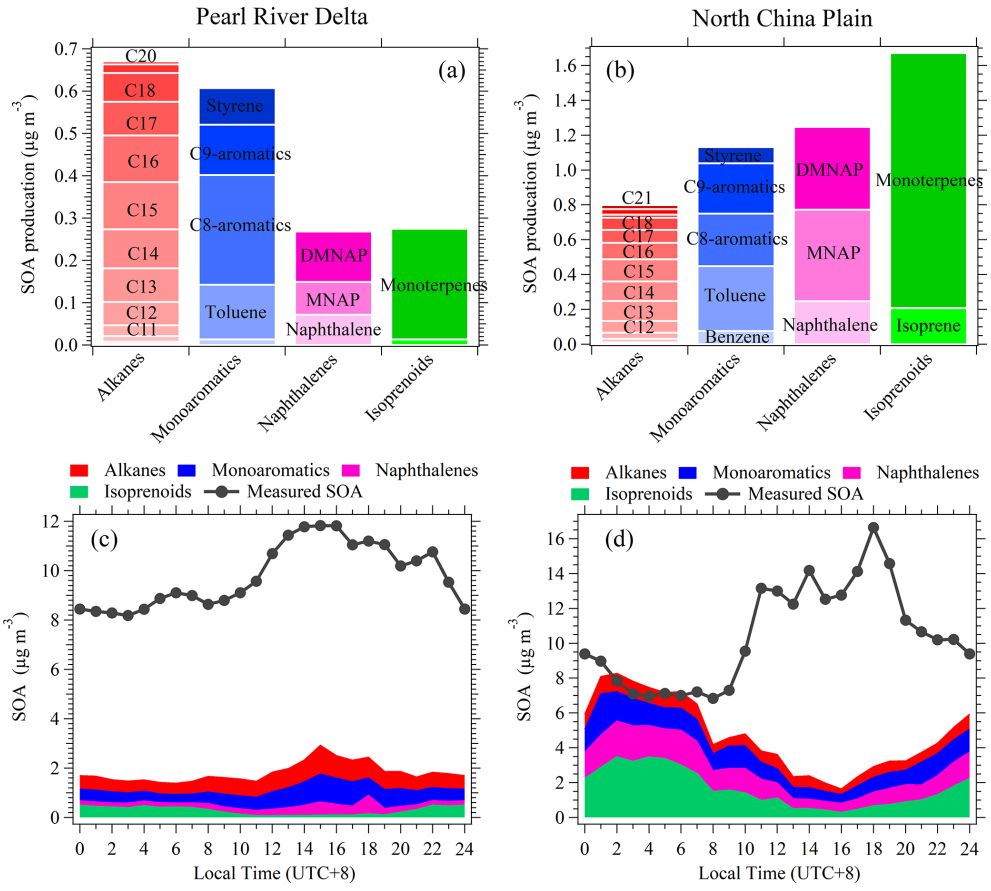

Figure 9. The mean concentrations of SOA produced from higher alkanes (C8–C21 alkanes), monoaromatics (benzene, toluene, C8 aromatics, C9 aromatics, and styrene), naphthalenes (naphthalene, methylnaphthalenes, and dimethylnaphthalenes), and isoprenoids (isoprene and monoterpenes) in PRD **(a)** and NCP **(b)**. Diurnal variations of SOA production from higher alkanes, monoaromatics, naphthalenes, and isoprenoids as well as the measured SOA concentrations in PRD **(c)** and NCP **(d)**.

concentrations from both *n*-alkanes and branched alkanes. With the total concentration of both *n*-alkanes and branched alkanes quantified, the contribution from higher alkanes at each carbon number can be estimated as a whole. This is an important supplementary method to the traditional analytical method by GC techniques for higher alkanes, as fully chemical separation and detection of numerous isomers of higher alkanes remain a challenge, even when using the most advanced GC × GC-ToF-MS instruments (Chan et al., 2013; Alam et al., 2016).

Higher alkanes were found to have significant contributions to SOA in both PRD and NCP regions, with contributions similar to or even higher that those of monoaromatics and naphthalenes. The importance of higher alkanes to SOA formation also calls for more work to investigate emissions and the chemistry of these compounds in the atmosphere. It was shown that fossil-related combustions such as vehicle exhaust are major sources of higher alkanes (Zhao et al., 2016). Recent studies have shown that non-combustion sources, such as the use of solvents, have a potentially significant impact on high-alkane emissions (McDonald et al., 2018; Khare and Gentner, 2018). However, such quantitative information on emissions of higher alkanes is still limited. The measurements of higher alkanes using NO^+ PTR-ToF-MS with a fast response could help to fill these research gaps.

Data availability. Data are available from the authors upon request.

Supplement. The supplement related to this article is available online at: https://doi.org/10.5194/acp-20-14123-2020-supplement.

Author contributions. BY and MS designed the research. CMW, CHW, SHW, JPQ, BLW, WC, CW, WS, and WYX contributed to data collection. CMW performed the data analysis, with contributions from ZLW, WWH, SXY, and CSY. CMW and BY prepared the manuscript with contributions from other authors. All the authors reviewed the manuscript.

Competing interests. The authors declare that they have no conflict of interest.

Acknowledgements. The authors gratefully acknowledge the science team for their technical support and discussions during the campaigns in PRD and NCP.

Financial support. This research has been supported by the Guangdong Provincial Key R & D Plan (grant no. 2019B110206001), the National Key R & D Plan of China (grant nos. 2019YFE0106300, 2018YFC0213904, and 2016YFC0202206), the National Natural Science Foundation of China (grant nos. 41877302 and 91644215), Guangdong Natural Science Funds for Distinguished Young Scholars (grant no. 2018B030306037), the Guangdong Soft Science Research Program (grant no. 2019B101001005), and the Guangdong Innovative and Entrepreneurial Research Team Program (grant no. 2016ZT06N263). This work was also supported by the Special Fund Project for Science and Technology Innovation Strategy of Guangdong Province (grant no. 2019B121205004). Weiwei Hu and Wei Chen were supported by the National Natural Science Foundation of China (grant no. 41875156) and Natural Science Foundation of Guangdong (grant no. 2019A1515011153).

Review statement. This paper was edited by Jason Surratt and reviewed by five anonymous referees.

References

Ahlberg, E., Falk, J., Eriksson, A., Holst, T., Brune, W. H., Kristensson, A., Roldin, P., and Svenningsson, B.: Secondary organic aerosol from VOC mixtures in an oxidation flow reactor, Atmos. Environ., 161, 210–220, https://doi.org/10.1016/j.atmosenv.2017.05.005, 2017.

Ait-Helal, W., Borbon, A., Sauvage, S., de Gouw, J. A., Colomb, A., Gros, V., Freutel, F., Crippa, M., Afif, C., Baltensperger, U., Beekmann, M., Doussin, J.-F., Durand-Jolibois, R., Fronval, I., Grand, N., Leonardis, T., Lopez, M., Michoud, V., Miet, K., Perrier, S., Prévôt, A. S. H., Schneider, J., Siour, G., Zapf, P., and Locoge, N.: Volatile and intermediate volatility organic compounds in suburban Paris: variability, origin and importance for SOA formation, Atmos. Chem. Phys., 14, 10439–10464, https://doi.org/10.5194/acp-14-10439-2014, 2014.

Alam, M. S., Stark, C., and Harrison, R. M.: Using Variable Ionization Energy Time-of-Flight Mass Spectrometry with Comprehensive GC × GC To Identify Isomeric Species, Anal. Chem., 88, 4211–4220, https://doi.org/10.1021/acs.analchem.5b03122, 2016.

Amador-Muñoz, O., Misztal, P. K., Weber, R., Worton, D. R., Zhang, H., Drozd, G., and Goldstein, A. H.: Sensitive detection of *n*-alkanes using a mixed ionization mode proton-transfer-reaction mass spectrometer, Atmos. Meas. Tech., 9, 5315–5329, https://doi.org/10.5194/amt-9-5315-2016, 2016.

An, Z., Huang, R. J., Zhang, R., Tie, X., Li, G., Cao, J., Zhou, W., Shi, Z., Han, Y., Gu, Z., and Ji, Y.: Severe haze in northern China: A synergy of anthropogenic emissions and atmospheric processes, P. Natl. Acad. Sci. USA, 116, 8657–8666, https://doi.org/10.1073/pnas.1900125116, 2019.

Anh, H. Q., Tomioka, K., Tue, N. M., Tuyen, L. H., Chi, N. K., Minh, T. B., Viet, P. H., and Takahashi, S.: A preliminary investigation of 942 organic micro-pollutants in the atmosphere in waste processing and urban areas, northern Vietnam: Levels, potential sources, and risk assessment, Ecotox. Environ. Safe, 167, 354–364, 2018.

Apel, E. C., Riemer, D. D., Hills, A., Baugh, W., Orlando, J., Faloona, I., Tan, D., Brune, W., Lamb, B., Westberg, H., Carroll, M. A., Thornberry, T., and Geron, C. D.: Measurement and interpretation of isoprene fluxes and isoprene, methacrolein, and methyl vinyl ketone mixing ratios at the PROPHET site during the 1998 Intensive, J. Geophys. Res.-Atmos., 107, ACH 7-1–ACH 7-15, https://doi.org/10.1029/2000JD000225, 2002.

Atkinson, R.: Kinetics of the gas-phase reactions of OH radicals with alkanes and cycloalkanes, Atmos. Chem. Phys., 3, 2233–2307, https://doi.org/10.5194/acp-3-2233-2003, 2003.

Atkinson, R., Arey, J., and Aschmann, S. M.: Atmospheric chemistry of alkanes: Review and recent developments, Atmos. Environ., 42, 5859–5871, https://doi.org/10.1016/j.atmosenv.2007.08.040, 2008.

Bahreini, R., Ervens, B., Middlebrook, A. M., Warneke, C., de Gouw, J. A., DeCarlo, P. F., Jimenez, J. L., Brock, C. A., Neuman, J. A., Ryerson, T. B., Stark, H., Atlas, E., Brioude, J., Fried, A., Holloway, J. S., Peischl, J., Richter, D., Walega, J., Weibring, P., Wollny, A. G., and Fehsenfeld, F. C.: Organic aerosol formation in urban and industrial plumes near Houston and Dallas, Texas, J. Geophys. Res.-Atmos., 114, D00F16, https://doi.org/10.1029/2008JD011493, 2009.

Bertram, T. H., Kimmel, J. R., Crisp, T. A., Ryder, O. S., Yatavelli, R. L. N., Thornton, J. A., Cubison, M. J., Gonin, M., and Worsnop, D. R.: A field-deployable, chemical ionization time-of-flight mass spectrometer, Atmos. Meas. Tech., 4, 1471–1479, https://doi.org/10.5194/amt-4-1471-2011, 2011.

Bi, X. H., Sheng, G. Y., Peng, P., Chen, Y. J., Zhang, Z. Q., and Fu, J. M.: Distribution of particulate- and vapor-phase *n*-alkanes and polycyclic aromatic hydrocarbons in urban atmosphere of Guangzhou, China, Atmos. Environ., 37, 289–298, https://doi.org/10.1016/s1352-2310(02)00832-4, 2003.

Carlton, A. G., Wiedinmyer, C., and Kroll, J. H.: A review of Secondary Organic Aerosol (SOA) formation from isoprene, Atmos. Chem. Phys., 9, 4987–5005, https://doi.org/10.5194/acp-9-4987-2009, 2009.

Caumo, S., Vicente, A., Custodio, D., Alves, C., and Vasconcellos, P.: Organic compounds in particulate and gaseous phase collected in the neighbourhood of an industrial complex in Sao Paulo (Brazil), Air Qual. Atmos. Hlth., 11, 271–283, https://doi.org/10.1007/s11869-017-0531-7, 2018.

Chan, A. W. H., Kautzman, K. E., Chhabra, P. S., Surratt, J. D., Chan, M. N., Crounse, J. D., Kürten, A., Wennberg, P. O., Flagan, R. C., and Seinfeld, J. H.: Secondary organic aerosol formation from photooxidation of naphthalene and alkylnaphthalenes: implications for oxidation of intermediate volatility organic compounds (IVOCs), Atmos. Chem. Phys., 9, 3049–3060, https://doi.org/10.5194/acp-9-3049-2009, 2009.

Chan, A. W. H., Isaacman, G., Wilson, K. R., Worton, D. R., Ruehl, C. R., Nah, T., Gentner, D. R., Dallmann, T. R., Kirchstetter, T. W., Harley, R. A., Gilman, J. B., Kuster, W. C., de Gouw, J.

A., Offenberg, J. H., Kleindienst, T. E., Lin, Y. H., Rubitschun, C. L., Surratt, J. D., Hayes, P. L., Jimenez, J. L., and Goldstein, A. H.: Detailed chemical characterization of unresolved complex mixtures in atmospheric organics: Insights into emission sources, atmospheric processing, and secondary organic aerosol formation, J. Geophys. Res.-Atmos., 118, 6783–6796, https://doi.org/10.1002/jgrd.50533, 2013.

Chowdhury, P. H., He, Q., Male, T. L., Brune, W. H., Rudich, Y., and Pardo, M.: Exposure of Lung Epithelial Cells to Photochemically Aged Secondary Organic Aerosol Shows Increased Toxic Effects, Environ. Sci. Tech. Lett., 5, 424–430, https://doi.org/10.1021/acs.estlett.8b00256, 2018.

Corbin, C. J., Othman, A. D., Allan, J., Worsnop, R. D., Haskins, D. J., Sierau, B., Lohmann, U., and Mensah, A.: Peak-fitting and integration imprecision in the Aerodyne aerosol mass spectrometer: effects of mass accuracy on location-constrained fits, Atmos. Meas. Tech., 8, 4615–4636, https://doi.org/10.5194/amt-8-4615-2015, 2015.

Cubison, M. J. and Jimenez, J. L.: Statistical precision of the intensities retrieved from constrained fitting of overlapping peaks in high-resolution mass spectra, Atmos. Meas. Tech., 8, 2333–2345, https://doi.org/10.5194/amt-8-2333-2015, 2015.

de Gouw, J. and Warneke, C.: Measurements of volatile organic compounds in the earths atmosphere using proton-transfer-reaction mass spectrometry, Mass Spectrom. Rev., 26, 223–257, https://doi.org/10.1002/mas.20119, 2007.

de Gouw, J. A., Brock, C. A., Atlas, E. L., Bates, T. S., Fehsenfeld, F. C., Goldan, P. D., Holloway, J. S., Kuster, W. C., Lerner, B. M., Matthew, B. M., Middlebrook, A. M., Onasch, T. B., Peltier, R. E., Quinn, P. K., Senff, C. J., Stohl, A., Sullivan, A. P., Trainer, M., Warneke, C., Weber, R. J., and Williams, E. J.: Sources of particulate matter in the northeastern United States in summer: 1. Direct emissions and secondary formation of organic matter in urban plumes, J. Geophys. Res.-Atmos., 113, D08301, https://doi.org/10.1029/2007jd009243, 2008.

de Gouw, J. A., Welsh-Bon, D., Warneke, C., Kuster, W. C., Alexander, L., Baker, A. K., Beyersdorf, A. J., Blake, D. R., Canagaratna, M., Celada, A. T., Huey, L. G., Junkermann, W., Onasch, T. B., Salcido, A., Sjostedt, S. J., Sullivan, A. P., Tanner, D. J., Vargas, O., Weber, R. J., Worsnop, D. R., Yu, X. Y., and Zaveri, R.: Emission and chemistry of organic carbon in the gas and aerosol phase at a sub-urban site near Mexico City in March 2006 during the MILAGRO study, Atmos. Chem. Phys., 9, 3425–3442, https://doi.org/10.5194/acp-9-3425-2009, 2009.

de Gouw, J. A., Middlebrook, A. M., Warneke, C., Ahmadov, R., Atlas, E. L., Bahreini, R., Blake, D. R., Brock, C. A., Brioude, J., Fahey, D. W., Fehsenfeld, F. C., Holloway, J. S., Le Henaff, M., Lueb, R. A., McKeen, S. A., Meagher, J. F., Murphy, D. M., Paris, C., Parrish, D. D., Perring, A. E., Pollack, I. B., Ravishankara, A. R., Robinson, A. L., Ryerson, T. B., Schwarz, J. P., Spackman, J. R., Srinivasan, A., and Watts, L. A.: Organic aerosol formation downwind from the Deepwater Horizon oil spill, Science, 331, 1295–1299, https://doi.org/10.1126/science.1200320, 2011.

Donahue, N. M., Robinson, A. L., Stanier, C. O., and Pandis, S. N.: Coupled partitioning, dilution, and chemical aging of semivolatile organics, Environ. Sci. Technol., 40, 2635–2643, https://doi.org/10.1021/es052297c, 2006.

Drozd, G. T., Zhao, Y., Saliba, G., Frodin, B., Maddox, C., Oliver Chang, M. C., Maldonado, H., Sardar, S., Weber, R. J., Robinson, A. L., and Goldstein, A. H.: Detailed Speciation of Intermediate Volatility and Semivolatile Organic Compound Emissions from Gasoline Vehicles: Effects of Cold-Starts and Implications for Secondary Organic Aerosol Formation, Environ. Sci. Technol., 53, 1706–1714, https://doi.org/10.1021/acs.est.8b05600, 2019.

Dzepina, K., Volkamer, R. M., Madronich, S., Tulet, P., Ulbrich, I. M., Zhang, Q., Cappa, C. D., Ziemann, P. J., and Jimenez, J. L.: Evaluation of recently-proposed secondary organic aerosol models for a case study in Mexico City, Atmos. Chem. Phys., 9, 5681–5709, https://doi.org/10.5194/acp-9-5681-2009, 2009.

Edney, E. O., Kleindienst, T. E., Jaoui, M., Lewandowski, M., Offenberg, J. H., Wang, W., and Claeys, M.: Formation of 2-methyl tetrols and 2-methylglyceric acid in secondary organic aerosol from laboratory irradiated isoprene/NO_X/SO_2/air mixtures and their detection in ambient $PM_{2.5}$ samples collected in the eastern United States, Atmos. Environ., 39, 5281–5289, https://doi.org/10.1016/j.atmosenv.2005.05.031, 2005.

Gentner, D. R., Isaacman, G., Worton, D. R., Chan, A. W. H., Dallmann, T. R., Davis, L., Liu, S., Day, D. A., Russell, L. M., Wilson, K. R., Weber, R., Guha, A., Harley, R. A., and Goldstein, A. H.: Elucidating secondary organic aerosol from diesel and gasoline vehicles through detailed characterization of organic carbon emissions, P. Natl. Acad. Sci. USA, 109, 18318–18323, https://doi.org/10.1073/pnas.1212272109, 2012.

Goldstein, A. H. and Galbally, I. E.: Known and Unexplored Organic Constituents in the Earth's Atmosphere, Environ. Sci. Technol., 41, 1514–1521, https://doi.org/10.1021/es072476p, 2007.

Gong, P., Wang, X., and Yao, T.: Ambient distribution of particulate- and gas-phase n-alkanes and polycyclic aromatic hydrocarbons in the Tibetan Plateau, Environ. Earth Sci., 64, 1703–1711, https://doi.org/10.1007/s12665-011-0974-3, 2011.

Gueneron, M., Erickson, M. H., VanderSchelden, G. S., and Jobson, B. T.: PTR-MS fragmentation patterns of gasoline hydrocarbons, Int. J. Mass Spectrom., 379, 97–109, https://doi.org/10.1016/j.ijms.2015.01.001, 2015.

Hallquist, M., Wenger, J. C., Baltensperger, U., Rudich, Y., Simpson, D., Claeys, M., Dommen, J., Donahue, N. M., George, C., Goldstein, A. H., Hamilton, J. F., Herrmann, H., Hoffmann, T., Iinuma, Y., Jang, M., Jenkin, M. E., Jimenez, J. L., Kiendler-Scharr, A., Maenhaut, W., McFiggans, G., Mentel, Th. F., Monod, A., Prévôt, A. S. H., Seinfeld, J. H., Surratt, J. D., Szmigielski, R., and Wildt, J.: The formation, properties and impact of secondary organic aerosol: current and emerging issues, Atmos. Chem. Phys., 9, 5155–5236, https://doi.org/10.5194/acp-9-5155-2009, 2009.

Hayes, P. L., Carlton, A. G., Baker, K. R., Ahmadov, R., Washenfelder, R. A., Alvarez, S., Rappenglück, B., Gilman, J. B., Kuster, W. C., de Gouw, J. A., Zotter, P., Prévôt, A. S. H., Szidat, S., Kleindienst, T. E., Offenberg, J. H., Ma, P. K., and Jimenez, J. L.: Modeling the formation and aging of secondary organic aerosols in Los Angeles during CalNex 2010, Atmos. Chem. Phys., 15, 5773–5801, https://doi.org/10.5194/acp-15-5773-2015, 2015.

Hellén, H., Tykkä, T., and Hakola, H.: Importance of monoterpenes and isoprene in urban air in northern Europe, Atmos. Environ., 59, 59–66, https://doi.org/10.1016/j.atmosenv.2012.04.049, 2012.

Hodzic, A., Jimenez, J. L., Madronich, S., Canagaratna, M. R., DeCarlo, P. F., Kleinman, L., and Fast, J.: Modeling organic aerosols in a megacity: potential contribution of semi-volatile and intermediate volatility primary organic compounds to secondary organic aerosol formation, Atmos. Chem. Phys., 10, 5491–5514, https://doi.org/10.5194/acp-10-5491-2010, 2010.

Huang, G., Liu, Y., Shao, M., Li, Y., Chen, Q., Zheng, Y., Wu, Z., Liu, Y., Wu, Y., Hu, M., Li, X., Lu, S., Wang, C., Liu, J., Zheng, M., and Zhu, T.: Potentially Important Contribution of Gas-Phase Oxidation of Naphthalene and Methylnaphthalene to Secondary Organic Aerosol during Haze Events in Beijing, Environ. Sci. Technol., 53, 1235–1244, https://doi.org/10.1021/acs.est.8b04523, 2019.

Inomata, S., Tanimoto, H., and Yamada, H.: Mass Spectrometric Detection of Alkanes Using NO^+ Chemical Ionization in Proton-transfer-reaction Plus Switchable Reagent Ion Mass Spectrometry, Chem. Lett., 43, 538–540, https://doi.org/10.1246/cl.131105, 2013.

Isaacman, G., Wilson, K. R., Chan, A. W. H., Worton, D. R., Kimmel, J. R., Nah, T., Hohaus, T., Gonin, M., Kroll, J. H., Worsnop, D. R., and Goldstein, A. H.: Improved Resolution of Hydrocarbon Structures and Constitutional Isomers in Complex Mixtures Using Gas Chromatography-Vacuum Ultraviolet-Mass Spectrometry, Anal. Chem., 84, 2335–2342, https://doi.org/10.1021/ac2030464, 2012.

Jathar, S. H., Gordon, T. D., Hennigan, C. J., Pye, H. O. T., Pouliot, G., Adams, P. J., Donahue, N. M., and Robinson, A. L.: Unspeciated organic emissions from combustion sources and their influence on the secondary organic aerosol budget in the United States, P. Natl. Acad. Sci. USA, 111, 10473–10478, https://doi.org/10.1073/pnas.1323740111, 2014.

Jiang, F., Liu, Q., Huang, X., Wang, T., Zhuang, B., and Xie, M.: Regional modeling of secondary organic aerosol over China using WRF/Chem, J. Aerosol Sci., 43, 57–73, https://doi.org/10.1016/j.jaerosci.2011.09.003, 2012.

Jimenez, J. L., Canagaratna, M. R., Donahue, N. M., Prevot, A. S. H., Zhang, Q., Kroll, J. H., DeCarlo, P. F., Allan, J. D., Coe, H., Ng, N. L., Aiken, A. C., Docherty, K. S., Ulbrich, I. M., Grieshop, A. P., Robinson, A. L., Duplissy, J., Smith, J. D., Wilson, K. R., Lanz, V. A., Hueglin, C., Sun, Y. L., Tian, J., Laaksonen, A., Raatikainen, T., Rautiainen, J., Vaattovaara, P., Ehn, M., Kulmala, M., Tomlinson, J. M., Collins, D. R., Cubison, M. J., Dunlea, E. J., Huffman, J. A., Onasch, T. B., Alfarra, M. R., Williams, P. I., Bower, K., Kondo, Y., Schneider, J., Drewnick, F., Borrmann, S., Weimer, S., Demerjian, K., Salcedo, D., Cottrell, L., Griffin, R., Takami, A., Miyoshi, T., Hatakeyama, S., Shimono, A., Sun, J. Y., Zhang, Y. M., Dzepina, K., Kimmel, J. R., Sueper, D., Jayne, J. T., Herndon, S. C., Trimborn, A. M., Williams, L. R., Wood, E. C., Middlebrook, A. M., Kolb, C. E., Baltensperger, U., and Worsnop, D. R.: Evolution of Organic Aerosols in the Atmosphere, Science, 326, 1525–1529, https://doi.org/10.1126/science.1180353, 2009.

Jobson, B. T., Alexander, M. L., Maupin, G. D., and Muntean, G. G.: On-line analysis of organic compounds in diesel exhaust using a proton transfer reaction mass spectrometer (PTR-MS), Int. J. Mass Spectrom., 245, 78–89, https://doi.org/10.1016/j.ijms.2005.05.009, 2005.

Jordan, A., Haidacher, S., Hanel, G., Hartungen, E., Herbig, J., Maerk, L., Schottkowsky, R., Seehauser, H., Sulzer, P., and Maerk, T. D.: An online ultra-high sensitivity Proton-transfer-reaction mass-spectrometer combined with switchable reagent ion capability (PTR+SRI-MS), Int. J. Mass Spectrom., 286, 32–38, https://doi.org/10.1016/j.ijms.2009.06.006, 2009.

Keyte, I. J., Harrison, R. M., and Lammel, G.: Chemical reactivity and long-range transport potential of polycyclic aromatic hydrocarbons – a review, Chem. Soc. Rev., 42, 9333–9391, https://doi.org/10.1039/c3cs60147a, 2013.

Khare, P. and Gentner, D. R.: Considering the future of anthropogenic gas-phase organic compound emissions and the increasing influence of non-combustion sources on urban air quality, Atmos. Chem. Phys., 18, 5391–5413, https://doi.org/10.5194/acp-18-5391-2018, 2018.

Kleindienst, T. E., Edney, E. O., Lewandowski, M., Offenberg, J. H., and Jaoui, M.: Secondary Organic Carbon and Aerosol Yields from the Irradiations of Isoprene and α-Pinene in the Presence of NO_x and SO_2, Environ. Sci. Technol., 40, 3807–3812, https://doi.org/10.1021/es052446r, 2006.

Kleindienst, T. E., Jaoui, M., Lewandowski, M., Offenberg, J. H., and Docherty, K. S.: The formation of SOA and chemical tracer compounds from the photooxidation of naphthalene and its methyl analogs in the presence and absence of nitrogen oxides, Atmos. Chem. Phys., 12, 8711–8726, https://doi.org/10.5194/acp-12-8711-2012, 2012.

Koss, A. R., Warneke, C., Yuan, B., Coggon, M. M., Veres, P. R., and de Gouw, J. A.: Evaluation of NO^+ reagent ion chemistry for online measurements of atmospheric volatile organic compounds, Atmos. Meas. Tech., 9, 2909–2925, https://doi.org/10.5194/amt-9-2909-2016, 2016.

Kuang, Y., He, Y., Xu, W., Yuan, B., Zhang, G., Ma, Z., Wu, C., Wang, C., Wang, S., Zhang, S., Tao, J., Ma, N., Su, H., Cheng, Y., Shao, M., and Sun, Y.: Photochemical Aqueous-Phase Reactions Induce Rapid Daytime Formation of Oxygenated Organic Aerosol on the North China Plain, Environ. Sci. Technol., 54, 3849–3860, https://doi.org/10.1021/acs.est.9b06836, 2020.

Lamkaddam, H., Gratien, A., Pangui, E., Cazaunau, M., Picquet-Varrault, B., and Doussin, J.-F.: High-NO_x Photooxidation of *n*-Dodecane: Temperature Dependence of SOA Formation, Environ. Sci. Technol., 51, 192–201, https://doi.org/10.1021/acs.est.6b03821, 2017.

Li, L., Tang, P., Nakao, S., Kacarab, M., and Cocker III, D. R.: Novel Approach for Evaluating Secondary Organic Aerosol from Aromatic Hydrocarbons: Unified Method for Predicting Aerosol Composition and Formation, Environ. Sci. Technol., 50, 6249–6256, https://doi.org/10.1021/acs.est.5b05778, 2016.

Liang, C., Pankow, J. F., Odum, J. R., and Seinfeld, J. H.: Gas/Particle Partitioning of Semivolatile Organic Compounds To Model Inorganic, Organic, and Ambient Smog Aerosols, Environ. Sci. Technol., 31, 3086–3092, https://doi.org/10.1021/es9702529, 1997.

Liggio, J., Li, S.-M., Hayden, K., Taha, Y. M., Stroud, C., Darlington, A., Drollette, B. D., Gordon, M., Lee, P., Liu, P., Leithead, A., Moussa, S. G., Wang, D., O'Brien, J., Mittermeier, R. L., Brook, J. R., Lu, G., Staebler, R. M., Han, Y., Tokarek, T. W., Osthoff, H. D., Makar, P. A., Zhang, J., L. Plata, D., and Gentner, D. R.: Oil sands operations as a large source of secondary organic aerosols, Nature, 534, 91–94, https://doi.org/10.1038/nature17646, 2016.

Lim, Y. B. and Ziemann, P. J.: Products and mechanism of secondary organic aerosol formation from reactions of *n*-alkanes with OH radicals in the presence of NO_x, Environ. Sci. Technol., 39, 9229–9236, https://doi.org/10.1021/es051447g, 2005.

Lim, Y. B., and Ziemann, P. J.: Effects of Molecular Structure on Aerosol Yields from OH Radical-Initiated Reactions of Linear, Branched, and Cyclic Alkanes in the Presence of NO_x, Environ. Sci. Technol., 43, 2328–2334, https://doi.org/10.1021/es803389s, 2009.

Loza, C. L., Craven, J. S., Yee, L. D., Coggon, M. M., Schwantes, R. H., Shiraiwa, M., Zhang, X., Schilling, K. A., Ng, N. L., Canagaratna, M. R., Ziemann, P. J., Flagan, R. C., and Seinfeld, J. H.: Secondary organic aerosol yields of 12-carbon alkanes, Atmos. Chem. Phys., 14, 1423–1439, https://doi.org/10.5194/acp-14-1423-2014, 2014.

Ma, P. K., Zhao, Y., Robinson, A. L., Worton, D. R., Goldstein, A. H., Ortega, A. M., Jimenez, J. L., Zotter, P., Prévôt, A. S. H., Szidat, S., and Hayes, P. L.: Evaluating the impact of new observational constraints on P-S/IVOC emissions, multi-generation oxidation, and chamber wall losses on SOA modeling for Los Angeles, CA, Atmos. Chem. Phys., 17, 9237–9259, https://doi.org/10.5194/acp-17-9237-2017, 2017.

McDonald, B. C., de Gouw, J. A., Gilman, J. B., Jathar, S. H., Akherati, A., Cappa, C. D., Jimenez, J. L., Lee-Taylor, J., Hayes, P. L., McKeen, S. A., Cui, Y. Y., Kim, S.-W., Gentner, D. R., Isaacman-VanWertz, G., Goldstein, A. H., Harley, R. A., Frost, G. J., Roberts, J. M., Ryerson, T. B., and Trainer, M.: Volatile chemical products emerging as largest petrochemical source of urban organic emissions, Science, 359, 760–764, https://doi.org/10.1126/science.aaq0524, 2018.

Ng, N. L., Kroll, J. H., Chan, A. W. H., Chhabra, P. S., Flagan, R. C., and Seinfeld, J. H.: Secondary organic aerosol formation from *m*-xylene, toluene, and benzene, Atmos. Chem. Phys., 7, 3909–3922, https://doi.org/10.5194/acp-7-3909-2007, 2007.

Pagonis, D., Krechmer, J. E., de Gouw, J., Jimenez, J. L., and Ziemann, P. J.: Effects of gas–wall partitioning in Teflon tubing and instrumentation on time-resolved measurements of gas-phase organic compounds, Atmos. Meas. Tech., 10, 4687–4696, https://doi.org/10.5194/amt-10-4687-2017, 2017.

Pandis, S. N., Paulson, S. E., Seinfeld, J. H., and Flagan, R. C.: Aerosol formation in the photooxidation of isoprene and β-pinene, Atmos. Environ. A, 25, 997–1008, https://doi.org/10.1016/0960-1686(91)90141-S, 1991.

Presto, A. A., Miracolo, M. A., Donahue, N. M., and Robinson, A. L.: Secondary organic aerosol formation from high-NO_x photooxidation of low volatility precursors: *n*-alkanes, Environ. Sci. Technol., 44, 2029–2034, https://doi.org/10.1021/es903712r, 2010.

Pye, H. O. T. and Pouliot, G. A.: Modeling the Role of Alkanes, Polycyclic Aromatic Hydrocarbons, and Their Oligomers in Secondary Organic Aerosol Formation, Environ. Sci. Technol., 46, 6041–6047, https://doi.org/10.1021/es300409w, 2012.

Roberts, J., Marchewka, M., Bertman, S., Goldan, P., Kuster, W., de Gouw, J., Warneke, C., Williams, E., Lerner, B., Murphy, P., Apel, E., and Fehsenfeld, F.: Analysis of the isoprene chemistry observed during the New England Air Quality Study (NEAQS) 2002 Intensive Experiment, J. Geophys. Res.-Atmos., 111, D23S12, https://doi.org/10.1029/2006JD007570, 2006.

Robinson, A. L., Donahue, N. M., Shrivastava, M. K., Weitkamp, E. A., Sage, A. M., Grieshop, A. P., Lane, T. E., Pierce, J. R., and Pandis, S. N.: Rethinking organic aerosols: Semivolatile emissions and photochemical aging, Science, 315, 1259–1262, https://doi.org/10.1126/science.1133061, 2007.

Sangiorgi, G., Ferrero, L., Perrone, M. G., Papa, E., and Bolzacchini, E.: Semivolatile PAH and n-alkane gas/particle partitioning using the dual model: up-to-date coefficients and comparison with experimental data, Environ. Sci. Pollut. R., 21, 10163–10173, https://doi.org/10.1007/s11356-014-2902-z, 2014.

Stark, H., Yatavelli, R. L. N., Thompson, S. L., Kimmel, J. R., Cubison, M. J., Chhabra, P. S., Canagaratna, M. R., Jayne, J. T., Worsnop, D. R., and Jimenez, J. L.: Methods to extract molecular and bulk chemical information from series of complex mass spectra with limited mass resolution, Int. J. Mass Spectrom., 389, 26–38, https://doi.org/10.1016/j.ijms.2015.08.011, 2015.

Tajuelo, M., Rodriguez, D., Teresa Baeza-Romero, M., Diaz-de-Mera, Y., Aranda, A., and Rodriguez, A.: Secondary organic aerosol formation from styrene photolysis and photooxidation with hydroxyl radicals, Chemosphere, 231, 276–286, https://doi.org/10.1016/j.chemosphere.2019.05.136, 2019.

Takekawa, H., Minoura, H., and Yamazaki, S.: Temperature dependence of secondary organic aerosol formation by photooxidation of hydrocarbons, Atmos. Environ., 37, 3413–3424, https://doi.org/10.1016/S1352-2310(03)00359-5, 2003.

Timonen, H., Cubison, M., Aurela, M., Brus, D., Lihavainen, H., Hillamo, R., Canagaratna, M., Nekat, B., Weller, R., Worsnop, D., and Saarikoski, S.: Applications and limitations of constrained high-resolution peak fitting on low resolving power mass spectra from the ToF-ACSM, Atmos. Meas. Tech., 9, 3263–3281, https://doi.org/10.5194/amt-9-3263-2016, 2016.

Tkacik, D. S., Presto, A. A., Donahue, N. M., and Robinson, A. L.: Secondary Organic Aerosol Formation from Intermediate-Volatility Organic Compounds: Cyclic, Linear, and Branched Alkanes, Environ. Sci. Technol., 46, 8773–8781, https://doi.org/10.1021/es301112c, 2012.

Worton, D. R., Isaacman, G., Gentner, D. R., Dallmann, T. R., Chan, A. W. H., Ruehl, C., Kirchstetter, T. W., Wilson, K. R., Harley, R. A., and Goldstein, A. H.: Lubricating Oil Dominates Primary Organic Aerosol Emissions from Motor Vehicles, Environ. Sci. Technol., 48, 3698–3706, https://doi.org/10.1021/es405375j, 2014.

Wu, C., Wang, C., Wang, S., Wang, W., Yuan, B., Qi, J., Wang, B., Wang, H., Wang, C., Song, W., Wang, X., Hu, W., Lou, S., Ye, C., Peng, Y., Wang, Z., Huangfu, Y., Xie, Y., Zhu, M., Zheng, J., Wang, X., Jiang, B., Zhang, Z., and Shao, M.: Measurement Report: important contributions of oxygenated compounds to emissions and chemistry of VOCs in urban air, Atmos. Chem. Phys. Discuss., https://doi.org/10.5194/acp-2020-152, in review, 2020.

Wu, L., Wang, X., Lu, S., Shao, M., and Ling, Z.: Emission inventory of semi-volatile and intermediate-volatility organic compounds and their effects on secondary organic aerosol over the Pearl River Delta region, Atmos. Chem. Phys., 19, 8141–8161, https://doi.org/10.5194/acp-19-8141-2019, 2019.

Xie, M., Hannigan, M. P., and Barsanti, K. C.: Gas/particle partitioning of *n*-alkanes, PAHs and oxygenated PAHs in urban Denver, Atmos. Environ., 95, 355–362, https://doi.org/10.1016/j.atmosenv.2014.06.056, 2014.

Yang, W., Li, J., Wang, M., Sun, Y., and Wang, Z.: A Case Study of Investigating Secondary Organic Aerosol Formation Pathways in Beijing using an Observation-based SOA Box Model, Aerosol Air Qual. Res., 18, 1606–1616, https://doi.org/10.4209/aaqr.2017.10.0415, 2018.

Yuan, B., Chen, W. T., Shao, M., Wang, M., Lu, S. H., Wang, B., Liu, Y., Chang, C. C., and Wang, B. G.: Measurements of ambient hydrocarbons and carbonyls in the Pearl River Delta (PRD), China, Atmos. Res., 116, 93–104, https://doi.org/10.1016/j.atmosres.2012.03.006, 2012.

Yuan, B., Hu, W. W., Shao, M., Wang, M., Chen, W. T., Lu, S. H., Zeng, L. M., and Hu, M.: VOC emissions, evolutions and contributions to SOA formation at a receptor site in eastern China, Atmos. Chem. Phys., 13, 8815–8832, https://doi.org/10.5194/acp-13-8815-2013, 2013.

Yuan, B., Koss, A. R., Warneke, C., Coggon, M., Sekimoto, K., and de Gouw, J. A.: Proton-Transfer-Reaction Mass Spectrometry: Applications in Atmospheric Sciences, Chem. Rev., 117, 13187–13229, https://doi.org/10.1021/acs.chemrev.7b00325, 2017.

Zhang, X., Cappa, C. D., Jathar, S. H., McVay, R. C., Ensberg, J. J., Kleeman, M. J., and Seinfeld, J. H.: Influence of vapor wall loss in laboratory chambers on yields of secondary organic aerosol, P. Natl. Acad. Sci. USA, 111, 5802–5807, https://doi.org/10.1073/pnas.1404727111, 2014.

Zhao, Y., Kreisberg, N. M., Worton, D. R., Teng, A. P., Hering, S. V., and Goldstein, A. H.: Development of anIn SituThermal Desorption Gas Chromatography Instrument for Quantifying Atmospheric Semi-Volatile Organic Compounds, Aerosol Sci. Tech., 47, 258–266, https://doi.org/10.1080/02786826.2012.747673, 2013.

Zhao, Y., Hennigan, C. J., May, A. A., Tkacik, D. S., de Gouw, J. A., Gilman, J. B., Kuster, W. C., Borbon, A., and Robinson, A. L.: Intermediate-Volatility Organic Compounds: A Large Source of Secondary Organic Aerosol, Environ. Sci. Technol., 48, 13743–13750, https://doi.org/10.1021/es5035188, 2014.

Zhao, Y., Nguyen, N. T., Presto, A. A., Hennigan, C. J., May, A. A., and Robinson, A. L.: Intermediate Volatility Organic Compound Emissions from On-Road Diesel Vehicles: Chemical Composition, Emission Factors, and Estimated Secondary Organic Aerosol Production, Environ. Sci. Technol., 49, 11516–11526, https://doi.org/10.1021/acs.est.5b02841, 2015.

Zhao, Y., Nguyen, N. T., Presto, A. A., Hennigan, C. J., May, A. A., and Robinson, A. L.: Intermediate Volatility Organic Compound Emissions from On-Road Gasoline Vehicles and Small Off-Road Gasoline Engines, Environ. Sci. Technol., 50, 4554–4563, https://doi.org/10.1021/acs.est.5b06247, 2016.

Zhu, J., Penner, J. E., Lin, G., Zhou, C., Xu, L., and Zhuang, B.: Mechanism of SOA formation determines magnitude of radiative effects, P. Natl. Acad. Sci. USA, 114, 12685–12690, https://doi.org/10.1073/pnas.1712273114, 2017.